



Sol-gel synthesis of low carbon content and low surface area Li₄Ti₅O₁₂/carbon black composite as high-rate anode materials for lithium ion battery

Journal:	<i>RSC Advances</i>
Manuscript ID:	RA-ART-06-2015-011586.R1
Article Type:	Paper
Date Submitted by the Author:	17-Aug-2015
Complete List of Authors:	Chang, Chien-Min; Chung Yuan Christian University, Chemistry Chen, Yi-Chih; Chung Yuan Christian University, Chemistry Ma, Wei-Lun; Chung Yuan Christian University, Chemistry Wang, Pin-Han; Chung Yuan Christian University, Chemistry Lee, Ching-Feng; Chung Yuan Christian University, Chemistry Chen, Hwang-Sheng; Chung Yuan Christian University, Chemistry Chen, yuiwhei; Chung Yuan Christian University, Chemistry



Journal Name

ARTICLE

Sol-gel synthesis of low carbon content and low surface area $\text{Li}_4\text{Ti}_5\text{O}_{12}$ /carbon black composite as high-rate anode materials for lithium ion battery

Received 00th January 20xx,
Accepted 00th January 20xx

DOI: 10.1039/x0xx00000x

www.rsc.org/

Chien-Min Chang,^a Yi-Chih Chen,^a Wei-Lun Ma,^a Pin-Han Wang,^a Ching-Feng Lee,^a Hwang-Sheng Chen^a and Yui Whei Chen-Yang^{*abc}

The $\text{Li}_4\text{Ti}_5\text{O}_{12}$ /carbon black composite anode materials (LTO/CB) with various amount of carbon black (CB) as an extra carbon source are synthesized by the sol-gel method. The SEM images show that the micron-sized clusters are formed by the $\text{Li}_4\text{Ti}_5\text{O}_{12}$ nanoparticles with diameters of 5 - 15 nm. The N_2 absorption/desorption measurements indicate that the total pore volume and pore size of LTO/CB with only 3.04 wt.% carbon content (LTO/CB-2) are significantly increased, favoring the electrochemical properties, and the surface area is only $3.64 \text{ m}^2 \text{ g}^{-1}$, benefitting the electrode processing. The discharge capacity of the LTO/CB-2 electrode in voltage range of 1 - 2.5 V at 1, 2 and 5 C rate is 221, 200 and 156 mAh g^{-1} , respectively, and even after 150 cycles, it retains 214 mAh g^{-1} at 1 C. Moreover, for coin full-cell testing, the discharge capacity for the (LTO/CB-2)/ LiFePO_4 battery at 0.2, 0.5 and 1 C is 152, 149 and 133 mAh g^{-1} , respectively. These are the highest capacities at the rate of 0.2 - 5 C among the carbon-contained LTO electrodes with low surface area for half-cell reported up to now, indicating that LTO/CB-2 is a promising high-rate anode material for use in high power lithium ion batteries.

1. Introduction

For rechargeable lithium ion batteries (LIBs), safety issues are concerned for applications, especially in large batteries for electric vehicles (EVs), hybrid electric vehicles (HEVs) and other load-leveling applications.¹⁻³ The carbonaceous anode materials commonly used currently have high resistance at the electrode/electrolyte interface for high-rate performance, leading to kinetic problems of LIBs.⁴ Spinel-type $\text{Li}_4\text{Ti}_5\text{O}_{12}$ (LTO) is promising as an anode material for LIB due to its very flat voltage plateau at around 1.55 V vs. Li/Li^+ , avoiding the reduction of electrolyte and its zero-strain in the cubic lattice during electrochemical cycling, resulting in good specific capacity and capacity retention.^{5,6} Although LTO is more stable and safer than carbonaceous materials like graphite, its poor intrinsic electronic conductivity ($< 10^{-13} \text{ S m}^{-1}$) leads to the low specific capacity and rate capability.^{7,8}

Doping metal ions like Al^{3+} , V^{5+} ,^{9,10} reducing the particle size¹¹⁻¹³ or containing conductive carbon have been commonly used to improve the intrinsic electronic conductivity and rate capability of LTO. For the later method, it is desired not only to

reduce the side reactions between the electrolyte and the electrode but also improve the kinetics of electrochemical reaction by increasing the electronic and ionic mobility simultaneously.^{14,15} Table 1 lists the electrochemical cycling data of the reported carbon-contained LTOs with different carbon sources.^{4,6,15-27} It is found that the electrochemical performance was varied with the synthesized method used, the carbon precursors, carbon content, and specific surface area of the carbon-contained LTOs and weight percentage of the active material in the electrode.²⁸⁻³¹ Among them, the one with the reduced graphene oxide (rGO) as the carbon source by the hydrothermal process gave the best capacity at 1 C (187 mAh g^{-1}).⁶ Nevertheless, considering the self-discharge rate and preparation of high active material loading electrode, its high surface area ($243 \text{ m}^2 \text{ g}^{-1}$) will be a significant drawback.^{32,33} Besides, the high cost of reduced graphene oxide and hydrothermal process are other disadvantages for practical use. Hence, it is still worth to pursuit a cost-effective preparation method with a good combination of facile synthesis method, low-cost carbon precursor and low carbon content to synthesize low surface area electrode materials with a good electrochemical property at high discharge rate for LIB.

In this study, we combine the benefit of sol-gel method and the merit of low-cost carbon source of carbon black to synthesize a series of low carbon contents (2.51 - 5.89 wt.%) nano-scale $\text{Li}_4\text{Ti}_5\text{O}_{12}$ /CB composite materials with low surface area ($1.43 - 3.64 \text{ m}^2 \text{ g}^{-1}$). The loading effect of carbon on the high-rate and cycle stability of the LTO/CB electrodes in the

^a Department of Chemistry, Chung Yuan Christian University, 200 Chung-Pei Rd., Chung-Li District, Tao-Yuan, Taiwan 32023, Republic of China. E-mail: yuiwhei@cycu.edu.tw; Fax: +886 3 265 3399; Tel: +886 3 265 3317

^b Center for Nanotechnology, Chung Yuan Christian University, 200 Chung-Pei Rd., Chung-Li District, Tao-Yuan, Taiwan 32023, Republic of China

^c Center for Biomedical Technology, Chung Yuan Christian University, 200 Chung-Pei Rd., Chung-Li District, Tao-Yuan, Taiwan 32023, Republic of China

Please do not adjust margins

ARTICLE

Journal Name

Table 1 Summary of electrochemical cycling data of the carbon-contained LTO samples with different carbon sources

Carbon Source	Carbon content (wt.%)	Surface area (m ² g ⁻¹)	Preparation method	The capacities in the voltage range of 1 - 2.5 V			Cyclic performance Capacity value; after “n” cycles	Ref.
				AM ^a (%)	Reversible capacity at C-rate (mAh g ⁻¹ @ C)			
Acetyl glucosamine	5.2	-	Solid state	80	160 @ 0.2 C;	146 @ 5 C	Capacity retention 96%, 154 @ 1 C; 1000	16
Sucrose@TiO ₂	5	-	Solid state	84	171 @ 0.2 C	150 @ 5 C	Capacity retention 98%, 150 @ 5 C; 300	17
Starch	3.2	-	Solid state	80	169 @ 0.2C;	142 @ 5C	157 @ 1C; 25	18
PAALi	4.8	-	Solid state	86	175 @ 0.86 mA cm ⁻²		Capacity retention 91 %, 130 @ 8.6 mA cm ⁻² ; 50	19
PEDOT	10	-	Hydrothermal	80	172 @ 0.2 C	135 @ 10 C	Capacity retention 99.5%, 169 @ 1 C; 100	20
rGO	1.2	234	Hydrothermal	80	187 @ 1 C;	160 @ 5 C	315 @ 1 C, the first cycle; 167 @ 1 C; 100	6
Graphene	5.9	-	Spray-dried	80	153 @ 0.5 C;	134 @ 5 C	Capacity retention 86 %, 124 @ 2 C; 2400	21
Graphite nanoplatlet	-	30	Super critical drying	75	147 @ 0.33 C		-	22
Citric acid	3.5	18.8	Sol-gel	85	174 @ 0.1 C;	101 @ 5 C	118 @ 1C; 50	23
PVP and F127	7.3	212	Sol-gel, electrospun	80	170 @ 0.1 C	105 @ 10 C	Capacity retention 96.3%, 123 @ 5 C; 100	24
Filter paper	-	-	Sol-gel	74	165 @ 0.2 C;	128 @ 6 C	Capacity retention 89 %, 116 @ 5 C; 470	15
LTO, CNT	15.2	-	Sol-gel	-	149 @ 0.2 C;	103 @ 10 C	-	25
MWNT@TiO ₂	17.5	80.1	Sol-gel	85	159 @ 1 C;	148 @ 5 C	Capacity retention 94% @ 1 C; 100	4
Graphene	7.2	173	Sol-gel, electrospun	70	164 @ 0.2 C;	137 @ 8 C	Capacity retention 91%, 101 @ 22 C; 1300	26
Graphene	7.8	-	Sol-gel	82	174 @ 0.2 C;	146 @ 10 C	110 @ 10 C; 100	27
Carbon black	3.0	3.6	Sol-gel	80	239 @ 0.2 C	156 @ 5 C	221 @ 1C; 50	This work

^a The weight percentage of active material in the electrode

Please do not adjust margins

voltage range of 1 - 2.5 V vs. Li/Li⁺ is studied in detail. The results indicate that the LTO/CB electrodes prepared are more cost-effective and higher rate capability carbon-contained LTO electrode materials than the others reported. Therefore, the LTO/CBs prepared in this study have high potential for application in the high power LIBs.

2. Experimental

2.1. Materials Preparation

The starting materials lithium acetate (CH₃COOLi, Alfa Aesar), carbon black (DENKA HS-100, specific surface area of 39 m² g⁻¹) (CB) and titanium isopropoxide (Ti(OCH(CH₃)₂)₄, 97 %, ALDRICH) were used as received. The carbon-contained spinel-type oxide Li₄Ti₅O₁₂ materials (C-LTOs), including LTO/C which was prepared without CB and LTO/CBs, were synthesized by the sol-gel method. Typically, 8.48 g of lithium acetate was dissolved in 30 g of ethanol and the designated amount of CB was added. Then 58.96 g of 50 wt.% titanium isopropoxide/isopropanol [(CH₃)₂CHOH, 99 %, ALDRICH] solution was mixed into it. After stirring for 20 min, the solution was set, allowed to gel, and aged for another 2 days. Finally, the wet gel obtained was dried and followed by calcination at 800 °C for 12 hours under N₂ gas. As listed in Table 2 the as-prepared C-LTOs were abbreviated as LTO/CB-1 to LTO/CB-4 with increasing the amount of CB from 2 to 5 wt.% based on the theoretical weight (0.02 mole, 9.19 g) of pristine Li₄Ti₅O₁₂. For comparison, the sample abbreviated as LTO/C was prepared without addition of CB by the same process.

2.2. Cell fabrication

The working electrodes consisted of 80 wt.% of the various active materials, C-LTOs, 10 wt.% conductive agent (DENKA HS-100), and 10 wt.% binder (polyvinylidene fluoride). All the electrodes were loaded with ca. 2.6 mg cm⁻² and punched into discs of ca. 10 mm diameter. Lithium foil was used both as a counter electrode and as a reference electrode in the coin half-cells. For the coin full-cell testing, except the as-prepared C-LTOs as the active anode material, LiFePO₄ (P13F, Tatum Fine Chemicals Co., Taiwan) was used as the active cathode material, LiPF₆ (1 mol L⁻¹) in a mixture of ethylene carbonate (EC)-propylene carbonate (PC)-diethyl carbonate (DEC) with a volume ratio EC-PC-DEC = 1: 1: 1 as the electrolyte and a polypropylene membrane (Celgard 2320) as the separator. The electrochemical properties were studied in the half-cell and full-cell with CR2032 coin cells assembled in an argon-filled glove box, where the H₂O and O₂ concentrations were less than 1 ppm.

2.3. Characterization

The structures of the C-LTOs were characterized on an X-ray diffraction spectroscopy (XRD), PANalytical X'Pert Pro MRD, with Cu K α radiation source ($\lambda = 1.5418 \text{ \AA}$). The carbon content in C-LTOs was determined by the element analyzer, Vario EL III.

The intrinsic electronic conductivity measurements were performed with a four-point probe connected to a Keithley 2400 voltmeter constant-current source system. The Raman spectra were obtained from Horiba triax320 using a He-Ne laser (632.8 nm). Nitrogen adsorption/desorption isotherms were determined on Micromeritics Tristar 3000. The scanning electron microscopy (SEM) images of C-LTOs were obtained at two magnifications (20kx and 100kx) using a JEOL JEM-7600F. The transmission electron microscopy (TEM) images and high resolution transmission electron microscopy energy dispersion spectroscopy (HRTEM-EDS) element mapping of C-LTOs were observed by JEOL JEM2000FX II and JEOL JEM2100, respectively. The X-Ray photoelectron spectroscopy (XPS) measurements were performed on Perkin Elmer PHI 5900.

Both cyclic voltammetry (CV) and electrochemical impedance spectroscopy (EIS) measurements were performed on AUTOLAB PGSTAT30. Cyclic voltammetry data was collected in the range of 1 - 2.5 V vs. Li/Li⁺ at the scan rate of 1 mV s⁻¹. EIS data was collected by applying AC amplitude of 5 mV over the frequency range of 10⁵ - 10⁻² Hz. Both rate capability and galvanostatic charge-discharge cycling tests were performed on Land CT2001A (5 V, 2 mA) in the range of 1 - 2.5 V. The C-rate was calculated from the weight and theoretical capacity of the C-LTO electrodes. Self-discharge studies were performed on Land CT2001A (5 V, 2 mA) and Keithley 2400. After the initial charging to 2.5 V at 0.2 C, the coin half-cells were stored at 25 °C for 28 days and their open-circuit potential (OCP) were measured each day. After storing for 28 days, the residual capacities of the coin half-cells were measured by discharging to 1 V at 0.2 C.

3. Results and Discussion

3.1. Characterization of the C-LTO samples

Although the carbon addition can increase intrinsic electronic conductivity of the active material, the capacity of the corresponding electrode is mainly contributed from the active material (LTO in this study); therefore, a limited carbon

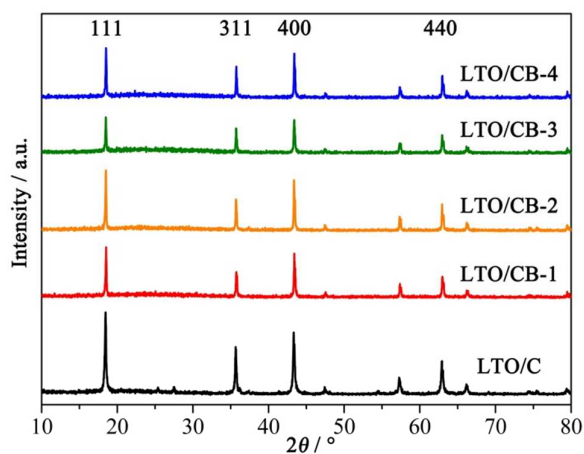


Fig. 1. XRD patterns of the C-LTO samples.

Table 2 Physical and textural properties of the C-LTO samples.

	LTO/C	LTO/CB-1	LTO/CB-2	LTO/CB-3	LTO/CB-4
Carbon					
CB addition / wt. %	0	2	3	4	5
Carbon content / wt. %	2.17	2.51	3.04	4.08	5.89
Lattice Parameter					
a / Å	8.3317	8.3114	8.3165	8.3194	8.3182
Intrinsic electronic conductivity					
$\kappa / 10^{-8} \text{ S cm}^{-1}$	3.8	16.6	11.7	11.1	6.8
Graphitization degree of C (GD)					
I_G/I_D	0.91	0.99	1.02	0.98	0.96
Textural properties					
Surface area / $\text{m}^2 \text{ g}^{-1}$	3.69	3.23	3.64	2.72	1.43
Average pore diameter / nm	13.85	26.70	33.15	39.33	46.51
Total pore volume / $\text{cm}^3 \text{ g}^{-1}$	0.010	0.023	0.030	0.020	0.022

content is desired for synthesis of high capacity anode material. Based on this concept and the carbon content reported (Table 1), 2 - 5 wt.% of CB of the LTO weight was added as the extra carbon source in this study. As listed in Table 2 the carbon content of LTO/C obtained by the EA measurement was 2.17 wt.%, resulted from calcination of the organic precursors, lithium acetate and titanium isopropoxide, during calcination in the inert gas. With increasing CB added (between 2 - 5 wt.%), the carbon content of LTO/CB prepared increased from 2.51 to 5.89 wt.%, which are less than most of the carbon-contained LTOs reported (Table 2).

Fig. 1 shows the XRD patterns of C-LTOs synthesized. The diffraction peaks of all C-LTOs are similar and assigned to $\text{Li}_4\text{Ti}_5\text{O}_{12}$ with a cubic spinel structure indexed to $Fd-3m$ space according to JCPDS card No-26-1198.³⁴ No obvious impure-phases and carbon are observed in these XRD patterns, implying low content and/or amorphous structure of carbon in these C-LTOs.³⁵ On the other hand, according to the Rietveld method, the lattice parameters were calculated from the XRD patterns using a Jade program, and listed in Table 2. The lattice parameters for LTO/CBs (8.3114 - 8.3194 Å) were only slightly smaller than that for LTO/C (8.3317 Å), indicating that the LTO's lattice size was barely changed.

3.2. Physical properties for the C-LTO samples

The intrinsic electronic conductivities (κ) of C-LTO powders were evaluated by the four-point probes DC method and the data are listed in Table 2. It is seen that the κ values of LTO/CBs (6.80×10^{-8} - $1.66 \times 10^{-7} \text{ S cm}^{-1}$) are all higher than that of LTO/C ($3.77 \times 10^{-8} \text{ S cm}^{-1}$), implying that the addition of CB enhanced the intrinsic electronic conductivity of LTO. However, the κ value was not proportional to the amount of CB added, revealing that the intrinsic electronic conductivity not simply depended on the carbon content but also related to the other factors such as graphitization degree of the carbon (GD) formed by calcination. As is known, the GD is proportional to the I_G/I_D ratio, a ratio of the intensities of the peaks at about 1610 cm^{-1} (G-band) and 1350 cm^{-1} (D-band) in its Raman Spectrum⁶. Table 2 indicates that the I_G/I_D ratio was

significantly increased from 0.91 for LTO/C to 0.99 for LTO/CB-1 and 1.02 for LTO/CB-2 then decreased to 0.98 and 0.96 for LTO/CB-3 and LTO/CB-4, respectively. The result indicates that although the carbon content was increased from LTO/CB-1 to LTO/CB-4, however the GD was decreased when the carbon content was more than 3.04 wt.%. Therefore, the κ value was significantly increased as carbon content was increased but was decreased after more carbon was contained. The result confirms that the intrinsic electronic conductivity of C-LTOs related to a combination of the carbon content and the graphitization degree of the carbon formed.

The textural properties of C-LTOs were measured by the N_2 adsorption/desorption isotherms and the data are listed in Table 2. As can be seen, the surface areas of C-LTOs (1.43 - $3.69 \text{ m}^2 \text{ g}^{-1}$) were all very low and similar because the surface area of CB added was small ($39 \text{ m}^2 \text{ g}^{-1}$) and the amount added were all less than 5 wt.%, which were much lower than those of the other carbon-contained LTOs reported.³⁶ The low surface areas of the electrode materials would avoid the possibility of poor adhesion with the collector and peeling off during the pressing and cutting processes, benefiting the preparation process of the electrode. On the other hand, the average pore diameter and total pore volume of LTO/CBs (26.70 - 46.51 nm and 0.020 - $0.030 \text{ cm}^3 \text{ g}^{-1}$) were all higher than that of LTO/C (13.85 nm and $0.010 \text{ cm}^3 \text{ g}^{-1}$). The average pore diameter was increased with increasing the carbon content. This might be caused by an increase in the particle size as the carbon content was increased. On the other hand, the total pore volume was significantly increased from $0.010 \text{ cm}^3 \text{ g}^{-1}$ for LTO/C to $0.023 \text{ cm}^3 \text{ g}^{-1}$ for LTO/CB-1 and $0.030 \text{ cm}^3 \text{ g}^{-1}$ for LTO/CB-2 then decreased to $0.020 \text{ cm}^3 \text{ g}^{-1}$ and $0.022 \text{ cm}^3 \text{ g}^{-1}$ for LTO/CB-3 and LTO/CB-4, respectively. The variation may be related to the size and the packing of the particles. The highest total pore volume obtained from LTO/CB-2 would favor the penetration of electrolyte, leading to an increase in the contact between the electrolyte and the electrode material and consequently, decreasing the resistance of the Li ion migration at the electrode/electrolyte interface.

3.3. Morphologies of the C-LTO samples

The SEM images of all C-LTOs are depicted in Fig. 2 at two magnifications (100k \times and 20k \times). The high magnification images in Fig. 2a-e exhibit that the clusters in the samples were all formed by the nano-sized particles (5 - 15 nm in diameter). This is similar to most of the materials synthesized by the sol-gel process¹¹ and is anticipated to result in the decrease of diffusion distance for the Li ions in the center of particle to the surface, profiting the Li ion insertion/desertion at high-rate. Besides, the sizes of the nanoparticles for part of LTO/CB-1 and other LTO/CBs were larger than that of LTO/C due to the presence of CB in the sol-gel process, implying that larger pores might be formed by these larger nanoparticles, benefiting to the penetration of the electrolyte. On the other hand, Fig. a'-e', the low magnification images, show that the gaps were created by the massive chunks formed by the aggregation of the micron-sized clusters. These gaps are also believed to benefit the penetration of the electrolyte, increasing the Li ion migration at the electrode/electrolyte interface.

The TEM image of LTO/C depicted in Fig. 3a clearly shows that LTO/C is composed of the primary particles with size of 5 - 15 nm, supporting the SEM result. The HRTEM-EDS element mapping of Ti and C for LTO/CB-2 are shown in Fig 3b and 3c, respectively. As can be seen, the Ti and C were uniformly distributed in the sample, implying that carbon dispersed in the sample well. The TEM image of LTO/CB-2 shown in Fig. 3d indicates that the lattice space of 0.48 nm corresponds to the interplanar spacing of (111) planes of the spinel $\text{Li}_4\text{Ti}_5\text{O}_{12}$ and the lattice fringe exhibits well-crystallinity. Besides, the amorphous carbon thin film in thickness of ca. 1 nm is found on the particle edge and is believed to be caused by the calcination of organic precursors and/or CB. The SAED pattern of LTO/CB-2 is depicted in Fig. 3e and displays a well-resolved concentric rings with bright spots, corresponding to the (111), (311), (400) and (333) diffraction planes of the spinel $\text{Li}_4\text{Ti}_5\text{O}_{12}$ and indicating that the particles are polycrystalline, which is in good agreement with the XRD result.

3.4. Cyclic voltammety performance of the C-LTO electrodes

The electrochemical properties of the Li ions inserting into and deserting out of the C-LTO electrodes were investigated by the coin cells with half-cell configuration. The cyclic voltammograms measured between 1 and 2.5 V vs. Li/Li^+ with a scan rate of 1 mV s^{-1} are shown in Fig. 4. The anodic (oxidation) peak potentials at about 1.78 - 1.83 V in the upper curve and the cathodic (reduction) peak potentials at about 1.47 - 1.49 V in the lower curve correspond to the redox couple of $\text{Ti}^{4+}/\text{Ti}^{3+}$ during the Li ions desertion and insertion process in the electrode, respectively. The potential difference between the anodic and cathodic peaks, i.e. electrode polarization, is about 291(LTO/C), 362(LTO/CB-1), 342(LTO/CB-2), 339(LTO/CB-3) and 338 mV (LTO/CB-4), respectively. Although these electrode polarizations of the LTO/CB electrodes were slightly larger than that of the LTO/C electrode, the current densities of the LTO/CB electrodes were

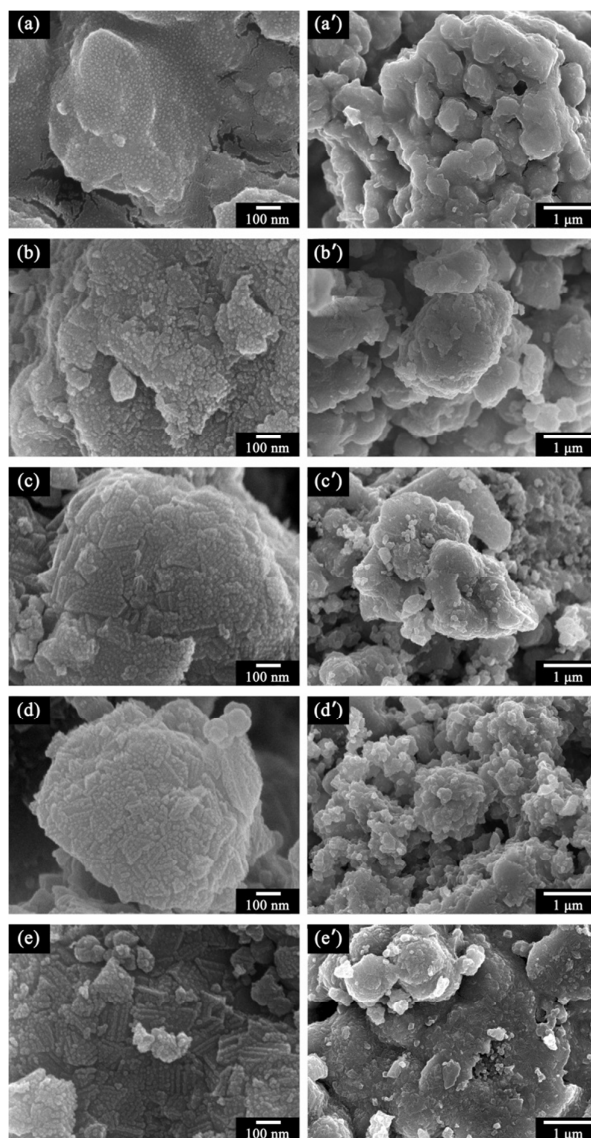


Fig. 2. SEM images of the C-LTO samples: (a, a') LTO/C, (b, b') LTO/CB-1, (c, c') LTO/CB-2, (d, d') LTO/CB-3, (e, e') LTO/CB-4 at 100k \times and 20k \times magnifications, respectively.

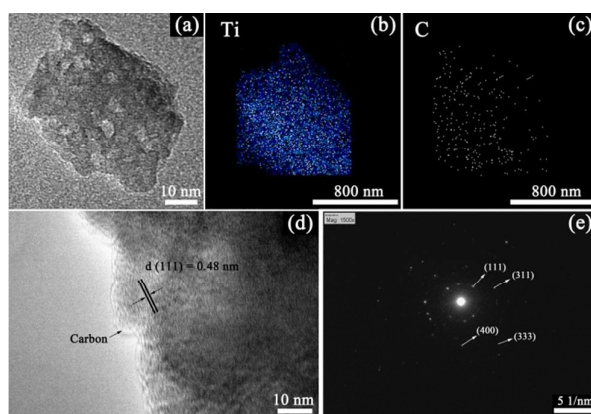


Fig. 3. (a) TEM image of LTO/C; /HRTEM-EDS element mapping of LTO/CB-2. (b) Ti, (c) C; (d) TEM image and (e) SAED pattern of LTO/CB-2.

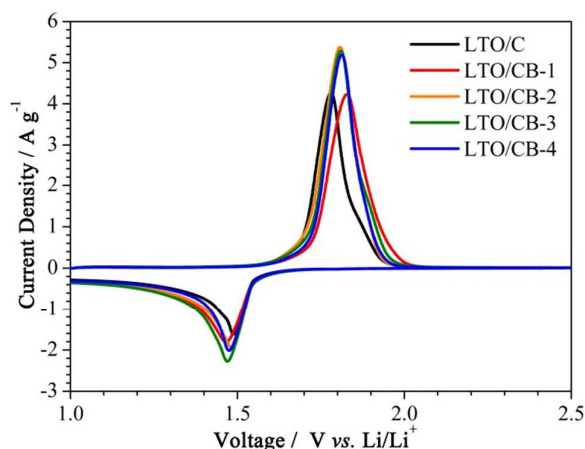


Fig. 4. Cyclic voltammogram properties in the voltage of 1 - 2.5 V for the C-LTO electrodes at a scan rate of 1 mV s^{-1} .

significantly higher than that of the LTO/C electrode, implying that the presence of CB did improve the electrochemical activities in the LTO/CB electrodes, especially for LTO/CB-2 to LTO/CB-4.

3.5. Rate capability and cyclic performance of the C-LTO electrodes

Fig. 5 shows the rate capability of the C-LTO electrodes in the voltage range of 1 - 2.5 V at various rates between 0.2 and 5 C. The discharge capacities of the LTO/C electrode were 188, 180, 166, 141 and 96 mAh g^{-1} at 0.2 C, 0.5 C, 1 C, 2 C and 5 C, respectively. It is slightly higher than the theoretical capacity of 175 mAh g^{-1} at 0.2 C and also better than that prepared with the solid state method (160 mAh g^{-1}).⁵ This is ascribed to the formation of nano-particles by the sol-gel process, leading to a larger contact area between the electrolyte and the electrode material and a shorter Li-ions diffusion distance.^{9, 37, 38} Even so, the discharge capacities of all the LTO/CB electrodes were all higher than that of the LTO/C electrode at all the rates between 0.2 and 5 C due to their higher conductivities and total pore volume caused by the addition of CB. Besides, all the capacities of the electrodes at 0.2 C measured after the cycling test from low-rate of 0.2 C to high-rate of 5 C are similar to the corresponding initial capacities measured at 0.2 C, confirming the zero-strain of C-LTOs in the cubic lattice that lead to the good capacity retention even at high-rate.

In addition, it is found that the capacities of all the LTO/CB electrodes measured at 0.2 C were higher than 200 mAh g^{-1} that was higher than the theoretical capacity (175 mAh g^{-1}). A similar result has been reported by Shao et al.,⁹ in which the higher capacity (216 mAh g^{-1} at 1 C) than the theoretical value was also obtained by the liquid formaldehyde treatment of $\text{Li}_4\text{Ti}_{4.85}\text{Al}_{0.15}\text{O}_{12}$ because 32 % of Ti^{4+} were reduced to Ti^{3+} . Besides, Wang et al.,⁶ also reported that a higher capacity (315 mAh g^{-1} at 1 C) than the theoretical value was obtained from the high surface area carbon-contained

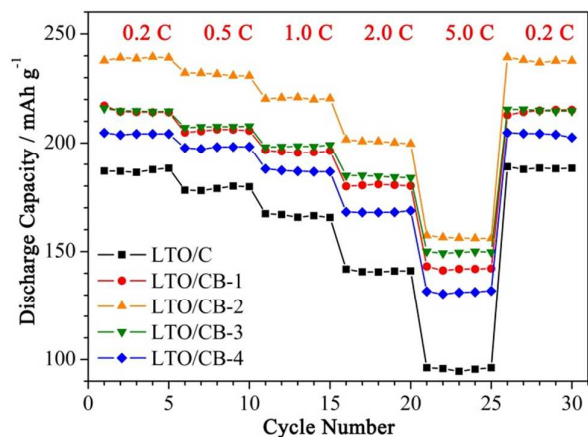


Fig. 5. Rate capabilities of the C-LTO electrodes at various rates between 0.2 and 5 C in 1 - 2.5 V.

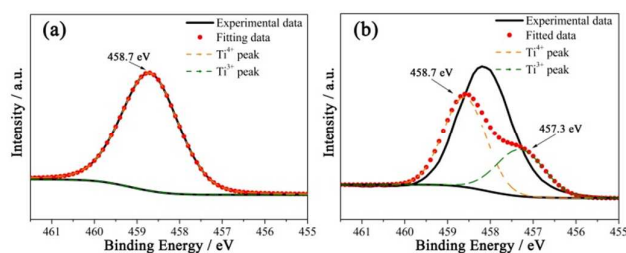


Fig. 6. Ti $2p_{3/2}$ XPS spectra of (a) LTO/C; (b) LTO/CB-2.

LTO, rGO-LTO. In this study, it is rationalized that due to the addition of CB, higher oxygen defect concentrations in LTO/CBs were obtained by the calcination under the inert gas, resulting in the generation of Ti^{3+} .^{6, 7} In order to confirm the generation of Ti^{3+} in LTO/CB-2, the Ti $2p_{3/2}$ XPS spectra of LTO/C and LTO/CB-2 were measured and shown in Fig. 6. As can be seen, the binding energy of Ti ions peaked at 458.7 eV for LTO/C and 458.1 eV for LTO/CB-2. By using the XPSPEAK program, the peaks were further deconvoluted into the binding energy peaks at about 458.7 and 457.3 eV for Ti^{4+} and Ti^{3+} , respectively.³⁹ It is observed that no Ti^{3+} peak is found in Fig. 6a, indicating that all the Ti ions were Ti^{4+} in LTO/C, while 27 % of Ti^{4+} were reduced to Ti^{3+} in LTO/CB-2 (Fig. 6b), which is similar to that reported by Shao et al.⁹ The result supports that the addition of CB not only increased the intrinsic electronic conductivity but also increased the amount of Ti^{4+} reduced to Ti^{3+} by the calcination under the inert gas. It is also worth to note that the highest capacities, 239 (0.2 C), 231 (0.5 C), 221 (1 C), 200 (2 C), 156 mAh g^{-1} (5 C), obtained from the LTO/CB-2 electrode are the highest capacity among the LTO/CBs prepared and higher than that of the other low surface area carbon-contained LTO electrodes reported. This demonstrates that LTO/CB-2 (with only 3.04 wt.% carbon content) prepared by the sol-gel method and the proper amount of CB as carbon source, provided the optimal condition for obtaining the best capacities between 0.2 C and 5 C charge-discharge rate in this study.

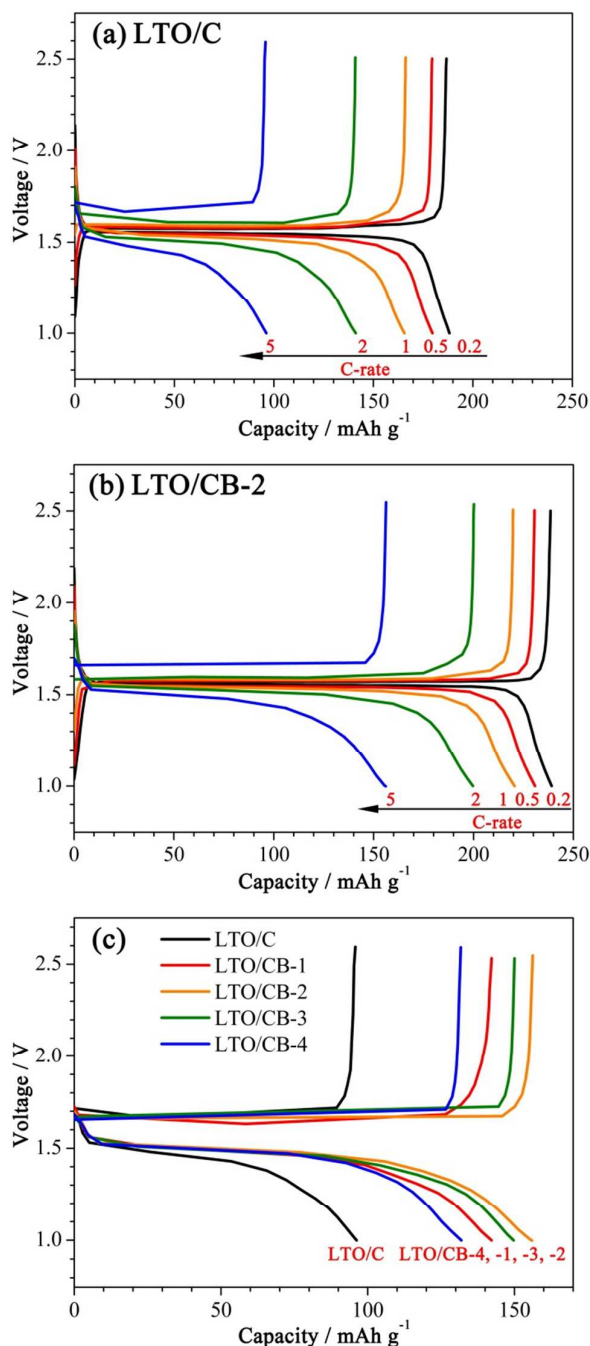


Fig. 7. Charge-discharge curves of the C-LTO electrodes in the voltage range of 1 - 2.5 V: (a) LTO/C electrode (b) LTO/CB-2 electrode at rates between 0.2 and 5 C; and (c) the C-LTO electrodes at 5 C.

Fig. 7a and 7b show the charge-discharge curves of rate capability for the LTO/C and LTO/CB-2 electrodes at various rates between 0.2 and 5 C. It can be seen that at 0.2 C the discharge plateaus appear at around 1.55 V vs. Li/Li⁺, corresponding to the redox of Ti⁴⁺/Ti³⁺ for both the LTO/C and LTO/CB-2 electrodes. As the rate was increased, the electrode polarization was increased, implying that less Li ions were able

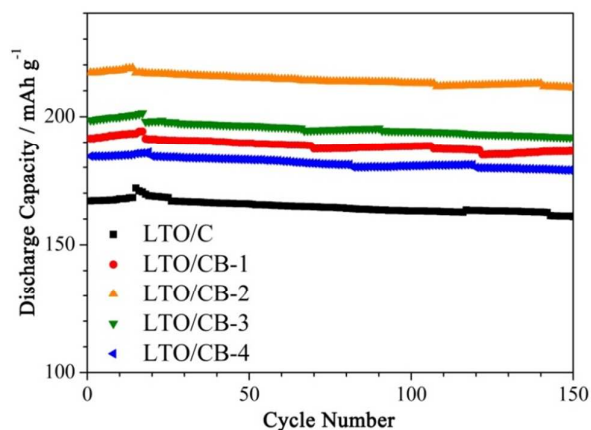


Fig. 8. Cyclic performances for the C-LTO electrodes at 1 C in the voltage range of 1 - 2.5 V.

to insert into and desert out of the electrodes at high-rate. Compared to the LTO/C electrode, the LTO/CB-2 electrode exhibited higher capacities and lower electrode polarization, implying easier Li ions migration in the LTO/CB-2 electrode than in the LTO/C electrode. Fig. 7c shows the charge-discharge curves of the C-LTO electrodes at the high rate of 5 C. As can be seen, all the LTO/CB electrodes exhibited much higher capacities and much lower electrode polarizations than the LTO/C electrode. The order of the trend is LTO/CB-2 > LTO/CB-3 > LTO/CB-1 > LTO/CB-4 > LTO/C.

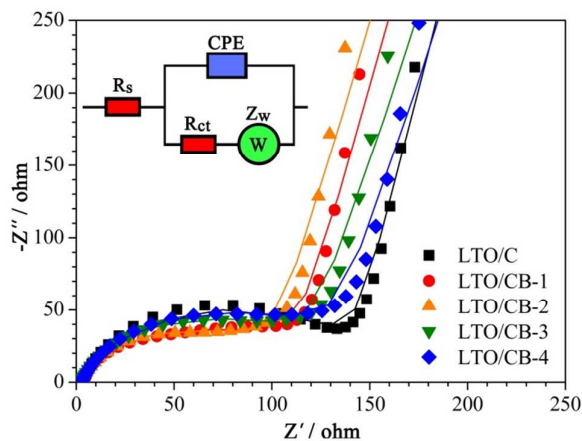
Fig. 8 shows the cyclic performances of the C-LTO electrodes at 1 C in the voltage range of 1 - 2.5 V. It exhibits good capacity retention for all the electrodes prepared, confirming the zero-strain of the cubic lattice during the cyclic performances. The fact that some of the 50th capacities of the C-LTO electrodes were slightly higher than the initial capacity is because the electrode was better penetrated by the electrolyte after several charge-discharge cycles. After 150 cycles, the capacity retentions of the C-LTO electrodes were 96.3% (LTO/C), 97.3% (LTO/CB-1), 97.3% (LTO/CB-2), 96.6% (LTO/CB-3) and 97.1% (LTO/CB-4), respectively. Furthermore, the LTO/CB-2 electrode had the highest capacity during all the 150 cycles, suggesting that the LTO/CB-2 electrode not only had the highest capacity but also had high retention in 150 cycles.

3.6. Electrochemical impedance spectroscopy

Fig. 9 shows the Nyquist plots of C-LTO electrodes and the equivalent circuit in the inset. The electrochemical impedance spectroscopy (EIS) results were fitted by the selected equivalent circuit using a ZView program and the impedance parameters are listed in Table 3. It shows that all the plots are comprised of a depressed semicircle in the high to medium frequency regions and a straight line in the low frequency region. The plot in the high frequency intercept at the real axis corresponds to the ohmic resistance of the cell and was mainly contributed from the electrolyte (R_s).⁴⁰ The semicircle in high to medium frequency region mainly represents the resistance

Table 3 Impedance parameters derived using equivalent circuit model of the LTO/C and LTO/CB-2 electrodes

Sample	R_s (Ω)	R_{ct} (Ω)	σ_w ($\Omega \text{ cm}^2 \text{ s}^{-1/2}$)	D_{Li} ($\text{cm}^2 \text{ s}^{-1}$)
LTO/C	3.02	120.5	119.32	2.11×10^{-13}
LTO/CB-1	2.44	84.1	93.12	3.47×10^{-13}
LTO/CB-2	2.35	74.7	97.05	3.20×10^{-13}
LTO/CB-3	2.27	99.5	103.87	2.79×10^{-13}
LTO/CB-4	3.37	108.3	106.70	2.64×10^{-13}

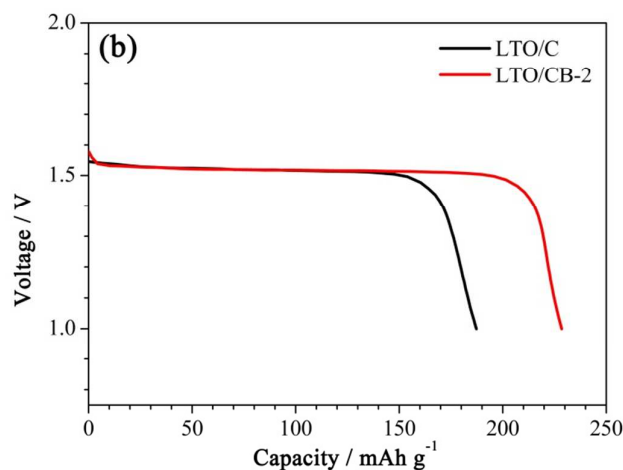
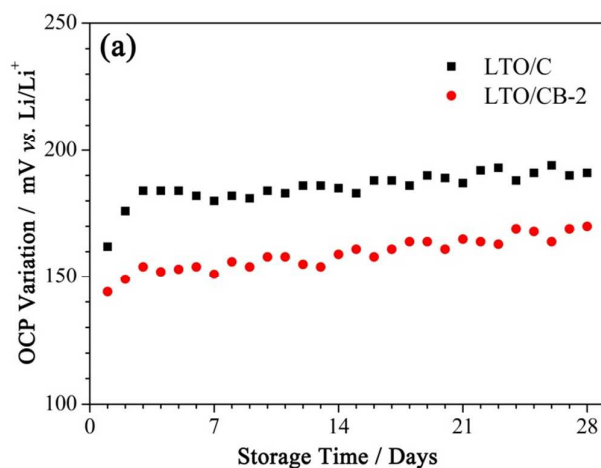
**Fig. 9.** Nyquist plots of the C-LTO electrodes and equivalent circuit inset.

in the migration of the Li ions at the electrode/electrolyte interface (R_{ct}) in parallel with a double-layer capacitance (CPE). The straight line in the low frequency region is attributed to the diffusion of the Li ions into the bulk of the electrode material, named Warburg diffusion (Z_w). As indicated in Table 3, the R_s values of the C-LTO electrodes are similar and much smaller than R_{ct} , revealing that R_{ct} was more critical than R_s for the Li ions transport. It is noticed that the R_{ct} value of the LTO/CB-2 electrode was the lowest among the electrodes prepared, revealing that the LTO/CB-2 electrode had the best migration of the Li ions at the electrode/electrolyte interface. This is ascribed to its higher pore volume. Moreover, EIS can be used to calculate the lithium diffusion coefficient (D_{Li}) of the Li ions diffusing into the electrode materials from Eq. (1) and the parameter of Warburg impedance coefficient (σ_w) can be calculated by Eq. (2)⁴¹

$$D_{Li} = R^2 T^2 / 2 A^2 n^4 F^4 C^2 \sigma_w^2 \quad (1)$$

$$Z_{re} = R_s + R_{ct} + \sigma_w \omega^{-1/2} \quad (2)$$

where Z_{re} is the real resistance of the cell, ω is angular frequency, R is the gas constant, T is the absolute temperature, A is the surface area of the electrode, n is the number of electrons transferred in the half-reaction for the redox couple, F is the Faraday constant, C is the concentration of Li ion in solid ($4.37 \times 10^{-3} \text{ mol cm}^{-3}$).⁴² Table 3 indicates that the Li ion diffusion coefficients of all the LTO/CB electrodes were higher than that of the LTO/C electrode, implying that the addition of CB in LTO benefited the Li ions diffusion in the electrode. However, the Li ion diffusion coefficient was decreased with increasing the carbon content. This is consistent with their intrinsic electronic conductivities discussed above. Even so,

**Fig. 10.** (a) Variation in OCP of the LTO/C and LTO/CB-2 electrodes for storage 28 days; (b) residual capacities at 0.2 C of the LTO/C and LTO/CB-2 electrodes after storage 28 days.

because the differences in the coefficients were all very small (in the order of -13), the performance of the C-LTO electrodes was mainly determined by R_{ct} . This result supports that the LTO/CB-2 electrode had the best performance mainly due to its lowest R_{ct} value.

The results confirm that the performance of the C-LTO electrodes related to a combination of the physical properties and textural properties of the C-LTO synthesized, and 3 wt.% in LTO/CB-2 was the optimal addition amount of CB for obtaining the best electrochemical properties in this study.

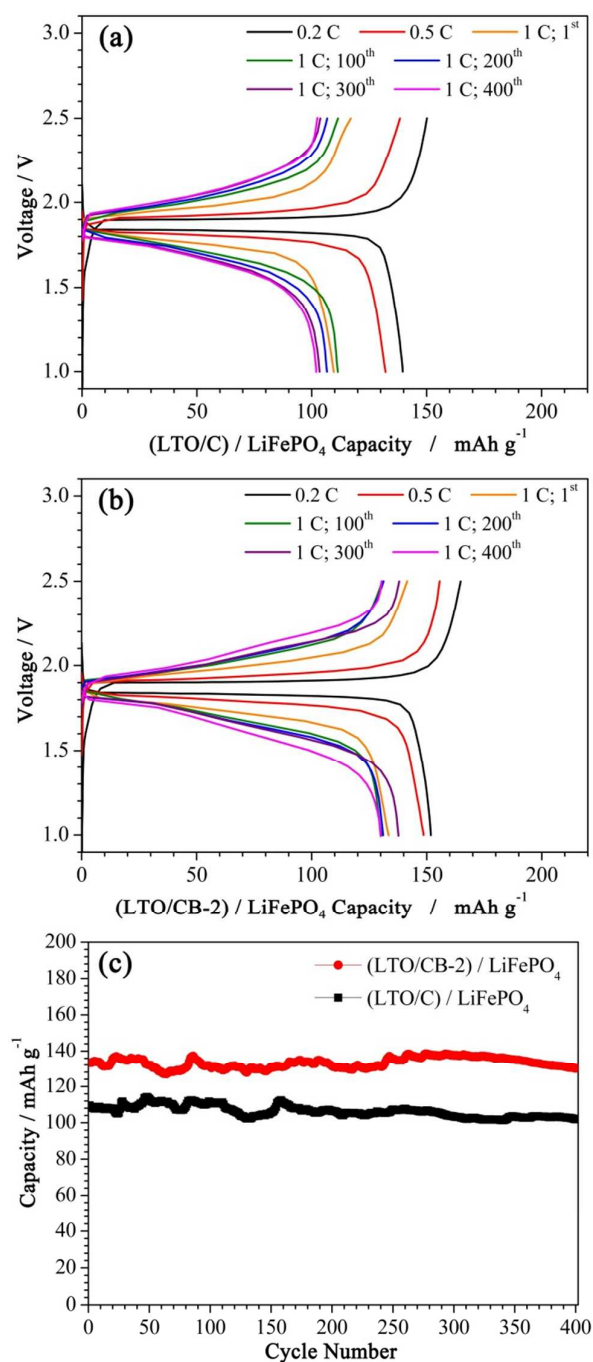


Fig. 11. Charge-discharge curves of: (a) (LTO/C)/LiFePO₄ battery; (b) (LTO/CB-2)/LiFePO₄ battery at 0.2 C for the 1st cycle, 0.5 C for the 2nd cycle and 1 C for the 1st, 100th, 200th, 300th and 400th cycles in the voltage range of 1 - 2.5 V. (c) cyclic performances of the (LTO/C)/LiFePO₄ and (LTO/CB-2)/LiFePO₄ batteries.

3.7. Self-discharge study

Fig. 10a shows the variation of open-circuit potential (OCP) for the LTO/C and LTO/CB-2 electrodes during storage for 28 days after the initial charging to 2.5 V at 0.2 C. As indicated in the figure, although the variation of OCP for both electrodes were less than 10% of its initial OCP value (1.748 V for LTO/C and 1.756 V for LTO/CB-2), the OCP variation of the LTO/CB-2

electrode (about 160 mV) is less than that of the LTO/C electrode (about 185 mV), implying that the LTO/CB-2 electrode was slightly better kept the optimal equilibrium between electrode and electrolyte⁴³. Besides, after the storage, the residual capacities of both electrodes were measured again by discharging to 1 V at 0.2 C and shown in Fig. 10b. The residual capacities for the LTO/C and LTO/CB-2 electrodes at 0.2 C were the same as their original capacities (187 mAh g⁻¹ and 227 mAh g⁻¹, respectively). This result indicates that the LTO/CB-2 electrode had slightly lower self-discharge rate electrode than the LTO-C electrode, indicating that LTO/CB-2 is a very promising anode material for storage and practical use in high power lithium ion batteries.⁴⁴

3.8. Coin full-cell electrochemical performance

Fig. 11a and 11b show the charge-discharge curves of the (LTO/C)/LiFePO₄ and (LTO/CB-2)/LiFePO₄ batteries at 1 C for the 1st, 100th, 200th, 300th and 400th cycles (before test at 1 C, the batteries were first cycled at 0.2 C and second cycled at 0.5 C) The C-rate was calculated from the weight and theoretical capacity of the LiFePO₄ cathode (170 mAh g⁻¹) for full-cell. It can be seen, the capacities of the (LTO/CB-2)/LiFePO₄ battery was higher than that of the (LTO/C)/LiFePO₄ battery and lower electrode polarization, especially at high-rate. Fig. 10c shows the cyclic performance of the (LTO/C)/LiFePO₄ and (LTO/CB-2)/LiFePO₄ batteries. The discharge capacities of the (LTO/C)/LiFePO₄ battery were 140, 132 mAh g⁻¹ at 0.2 C, 0.5 C, respectively and average discharge capacity of 106 mAh g⁻¹ at 1 C for 400 cycles. Compared to the (LTO/C)/LiFePO₄ battery, the discharge capacities of the (LTO/CB-2)/LiFePO₄ battery were all higher than that of the (LTO/C)/LiFePO₄ battery at the various rates. Furthermore, it is worth to note that the higher capacities, 152 (0.2 C), 149 (0.5 C) and 133 mAh g⁻¹ (1 C), were obtained from the (LTO/CB-2)/LiFePO₄ battery, confirming that the addition of CB benefited the Li ions diffusion into LTO in the full-cell. Even after 400 cycles, both the (LTO/C)/LiFePO₄ and (LTO/CB-2)/LiFePO₄ batteries kept good capacity retention as reported by Jagannathan et al.,⁴⁵ which demonstrated that the batteries composed of spinel Li₄Ti₅O₁₂ anode and olivine LiFePO₄ cathode were very stable because their structure had not been collapsed during the Li ions insertion and desertion process in the electrode.

Conclusions

In this study, the low carbon content Li₄Ti₅O₁₂ materials (LTO/CBs) were successfully synthesized by sol-gel method with the cheaper CB as the extra carbon source. The EA and DC four-point probes measurements showed that the low carbon contents (2.51 - 5.89 wt.%) LTO/CBs exhibited higher intrinsic electronic conductivities than LTO/C, which was prepared without CB. The N₂ absorption/desorption results showed that all LTO/CBs had low surface area (1.43 - 3.64 m² g⁻¹), larger pore volume and pore diameters, benefiting the penetration of the electrolyte. The SEM images showed that the micron-sized clusters were formed by the Li₄Ti₅O₁₂ nanoparticles with

diameters of 5 - 15 nm. The rate capability tests showed that the best discharge capacity was obtained from the LTO/CB-2 electrode in the voltage range of 1 - 2.5 V at 0.2, 0.5, 1, 2 and 5C with 239, 231, 221, 200 and 156 mAh g⁻¹, respectively. Even after 150 cycles, its capacity was 214 mAh g⁻¹ at 1 C and kept good cyclic performance. Besides, the detail EIS investigation indicated that the LTO/CB-2 electrode had lower charge transfer resistance, leading to the excellent electrochemical properties at high-rate. The result of the coin full-cell testing showed that the average capacity of 133 mAh g⁻¹ at 1 C obtained from the (LTO/CB-2)/LiFePO₄ battery was higher than that for the (LTO/C)/LiFePO₄ battery (106 mAh g⁻¹). It implies that the combination of the sol-gel method, the proper amount of CB, and the process condition not only made LTO/CB-2 the best anode material in this study but also better than the results of the other low surface area carbon-contained LTO anode materials reported up to now and is a high potential anode material for use in lithium ion battery practically.

Acknowledgements

The authors gratefully acknowledge the Ministry of Science and Technology, Taiwan, R.O.C. and Chung Yuan Christian University for supporting this research work under grant number: NSC 103-2113-M-033-002-MY3.

References

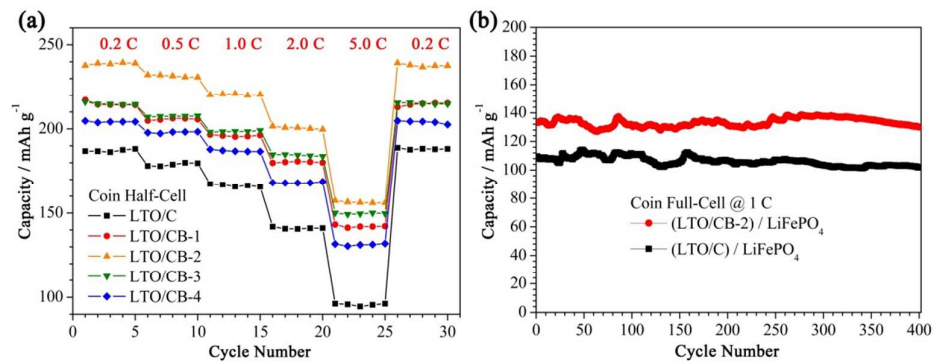
1. S. M. Rezvanizani, Z. Liu, Y. Chen and J. Lee, *J. Power Sources*, 2014, **256**, 110-124.
2. N. Takami, H. Inagaki, Y. Tatebayashi, H. Saruwatari, K. Honda and S. Egusa, *J. Power Sources*, 2013, **244**, 469-475.
3. V. Etacheri, R. Marom, R. Elazari, G. Salitra and D. Aurbach, *Energy Environ. Sci.*, 2011, **4**, 3243-3262.
4. L. Shen, C. Yuan, H. Luo, X. Zhang, K. Xu and F. Zhang, *J. Mater. Chem.*, 2011, **21**, 761-767.
5. T. Ohzhku, A. Ueda and N. Yamamoto, *J. Electrochem. Soc.*, 1995, **142**, 1431-1435.
6. C. Chen, Y. Huang, H. Zhang, X. Wang, G. Li, Y. Wang, L. Jiao and H. Yuan, *J. Power Sources*, 2015, **278**, 693-702.
7. X. Chen, X. Guan, L. Li and G. Li, *J. Power Sources*, 2012, **210**, 297-302.
8. C. H. Chen, J. T. Vaughey, A. N. Jansen, D. W. Dees, A. J. Kahaian, T. Goacher and M. M. Thackeray, *J. Electrochem. Soc.*, 2001, **148**, A102-A104.
9. R. Cai, S. Jiang, X. Yu, B. Zhao, H. Wang and Z. Shao, *J. Mater. Chem.*, 2012, **22**, 8013-8021.
10. C.-M. Chang, Y.-C. Chen, W.-L. Ma and Y. W. Chen-Yang, *RSC Adv.*, 2015, **5**, 49248-49256.
11. Y. Wu, M. V. Reddy, B. V. R. Chowdari and S. Ramakrishna, *Electrochim. Acta*, 2012, **67**, 33-40.
12. C.-H. Hong, A. Noviyanto, J. H. Ryu, J. Kim and D.-H. Yoon, *Ceram. Int.*, 2012, **38**, 301-310.
13. A. Guerfi, P. Charest, K. Kinoshita, M. Perrier and K. Zaghib, *J. Power Sources*, 2004, **126**, 163-168.
14. T.-F. Yi, L.-J. Jiang, J. Shu, C.-B. Yue, R.-S. Zhu and H.-B. Qiao, *J. Phys. Chem. Solids* 2010, **71**, 1236-1242.
15. G. Xie, J. Ni, X. Liao and L. Gao, *Mater. Lett.*, 2012, **78**, 177-179.
16. H. Li, L. Shen, X. Zhang, J. Wang, P. Nie, Q. Che and B. Ding, *J. Power Sources*, 2013, **221**, 122-127.
17. X. Guo, H. F. Xiang, T. P. Zhou, X. K. Ju and Y. C. Wu, *Electrochim. Acta*, 2014, **130**, 470-476.
18. L. Wang, Z. Zhang, G. Liang, X. Ou and Y. Xu, *Powder Technol.*, 2012, **215-216**, 79-84.
19. Z. Lin, X. Hu, Y. Huai, L. Liu, Z. Deng and J. Suo, *Solid State Ionics*, 2010, **181**, 412-415.
20. X. Wang, L. Shen, H. Li, J. Wang, H. Dou and X. Zhang, *Electrochim. Acta*, 2014, **129**, 283-289.
21. Z. Jian, L. Zhao, R. Wang, Y.-S. Hu, H. Li, W. Chen and L. Chen, *RSC Adv.*, 2012, **2**, 1751-1754.
22. R. P. Maloney, H. J. Kim and J. S. Sakamoto, *ACS Appl. Mater. Interfaces*, 2012, **4**, 2318-2321.
23. J. Wang, X.-M. Liu, H. Yang and X.-d. Shen, *J. Alloys Compd.*, 2011, **509**, 712-718.
24. J. Wang, L. Shen, H. Li, B. Ding, P. Nie, H. Dou and X. Zhang, *J. Alloys Compd.*, 2014, **587**, 171-176.
25. J. Shu, L. Hou, R. Ma, M. Shui, L. Shao, D. Wang, Y. Ren and W. Zheng, *RSC Adv.*, 2012, **2**, 10306-10309.
26. N. Zhu, W. Liu, M. Xue, Z. Xie, D. Zhao, M. Zhang, J. Chen and T. Cao, *Electrochim. Acta*, 2010, **55**, 5813-5818.
27. H. Xiang, B. Tian, P. Lian, Z. Li and H. Wang, *J. Alloys Compd.*, 2011, **509**, 7205-7209.
28. Y. Lin, M. X. Gao, D. Zhu, Y. F. Liu and H. G. Pan, *J. Power Sources*, 2008, **184**, 444-448.
29. G. Liu, H. Zheng, S. Kim, Y. Deng, A. M. Minor, X. Song and V. S. Battaglia, *J. Electrochem. Soc.*, 2008, **155**, A887-A892.
30. S. Yang, X. Zhou, J. Zhang and Z. Liu, *J. Mater. Chem.*, 2010, **20**, 8086-8091.
31. A. Mahmoud, J. M. Amarilla, K. Lasri and I. Saadoun, *Electrochim. Acta*, 2013, **93**, 163-172.
32. J. Wu, G. K. Dathar, C. Sun, M. G. Theivanayagam, D. Applestone, A. G. Dylla, A. Manthiram, G. Henkelman, J. B. Goodenough and K. J. Stevenson, *Nanotechnology*, 2013, **24**, 424009.
33. T. Utsunomiya, O. Hatozaki, N. Yoshimoto, M. Egashira and M. Morita, *J. Power Sources*, 2011, **196**, 8598-8603.
34. J.-Y. Lin, C.-C. Hsu, H.-P. Ho and S.-H. Wu, *Electrochim. Acta*, 2013, **87**, 126-132.
35. Y. Q. Qiao, X. L. Wang, J. Y. Xiang, D. Zhang, W. L. Liu and J. P. Tu, *Electrochim. Acta*, 2011, **56**, 2269-2275.
36. B. Z. Li, Y. Wang, L. Xue, X. P. Li and W. S. Li, *J. Power Sources*, 2013, **232**, 12-16.
37. B. Tian, H. Xiang, L. Zhang, Z. Li and H. Wang, *Electrochim. Acta*, 2010, **55**, 5453-5458.
38. Z. Yu, X. Zhang, G. Yang, J. Liu, J. Wang, R. Wang and J. Zhang, *Electrochim. Acta*, 2011, **56**, 8611-8617.
39. C. D. Wagner, W. M. Riggs, L. E. Davies, J. F. Moulder and G. E. Muilenberg, *Handbook of X-ray Photoelectron Spectroscopy*, Perkin-Elmer, Eden Prairie, MN, 1979.
40. C. Lin, X. Fan, Y. Xin, F. Cheng, M. O. Lai, H. Zhou and L. Lu, *Nanoscale*, 2014, **6**, 6651-6660.
41. B. Jin, E. M. Jin, K.-H. Park and H.-B. Gu, *Electrochem. Commun.*, 2008, **10**, 1537-1540.
42. S.-L. Chou, J.-Z. Wang, H.-K. Liu and S.-X. Dou, *J. Phys. Chem. C*, 2011, **115**, 16220-16227.
43. T. Utsunomiya, O. Hatozaki, N. Yoshimoto, M. Egashira and M. Morita, *J. Power Sources*, 2011, **196**, 8598-8603.

Journal Name

ARTICLE

44. T. Utsunomiya, O. Hatozaki, N. Yoshimoto, M. Egashira and M. Morita, *J. Power Sources*, 2011, **196**, 8675-8682.
45. P. Manikandan, P. Periasamy and R. Jagannathan, *J. Mater. Chem. A*, 2013, **1**, 15397-15405.

Graphical Abstract



(a) the rate capability performances of coin half-cells and (b) the cyclic performances of the coin full-cells. 3 wt.% in LTO/CB-2 is the optimal addition amount of CB for obtaining the best electrochemical properties in this study.